Polariton-plasmon coupling and Purcell-Dicke ultraradiance in a slab geometry

Jamal T. Manassah*
Department of Electrical Engineering, City College of New York, New York, New York 10031, USA
(Received 16 July 2013; published 6 November 2013)

The enhanced cooperative decay rate and the enhanced cooperative Lamb shift from a slab of two-level atoms placed in between two noble-metal slabs are analyzed within the context of the interacting polariton of the resonant medium and the metallic plasmon eigenmodes.

DOI: 10.1103/PhysRevA.88.053805 PACS number(s): 42.50.Nn

I. INTRODUCTION

Research on super-radiance investigates the enhancement in the decay rate of a collection of atoms coherently radiating. For an ensemble of N two-level atoms occupying a region of space whose dimension is much smaller than the wavelength of the atomic transition, in a seminal paper [1], Dicke predicted that the atomic ensemble's decay rate increases by a factor of N as compared to that of the isolated atom decay rate. This paper was extended to arbitrary sample size for different geometries (see Ref. [2] for a recent review). The expressions for this cooperative decay rate (CDR) and of the associated cooperative Lamb shift (CLS) for an ensemble of atoms in a slab's geometry was obtained in Ref. [3] and was experimentally verified in Ref. [4].

The extensive theoretical and experimental work on cavity electrodynamics (see Ref. [5] for a review) exploring the enhancement of the radiation rate from an atom in a cavity was developed based on the seminal work of Purcell [6] who was the first to investigate the enhancement of the radiative decay rate of a quantum system when in the close vicinity of a metallic conductor.

More recently, Friedberg and the author showed that the above-described physical effects can combine to further enhance the CDR of two-level atoms in spherical and one-dimensional geometries [7–9] when the metal plasmonic resonance frequency is equal to the atomic medium resonance frequency.

In this paper, I will further examine the Purcell-Dicke ultraradiance (this term is used to indicate that, in this case, we have a larger decay rate than that in traditional superradiance) from a slab of two-level atoms if these were placed between two noble-metal conductors within the context of the resonant polariton-plasmon modes coupling between the two-level medium bare mode with that of the metal bare mode.

The novelties in this paper as compared to our work in Refs. [7–9] are as follows: (i) Qualitatively, I show the reason for the existence of a limit on the Purcell enhancement factor or, equivalently, the reason for the existence of an upper limit on the ultraradiance cooperative decay rate and the reason for having the cooperative Lamb shift continuing to increase its value even after the CDR reached its limit; and (ii) quantitatively, I compute this CDR limit and the dependence of the enhanced CLS on the number density of the atomic medium in the region of saturation of the CDR value.

In Sec. II, I compute the transfer matrix for the present configuration. In Sec. III, I compute the transmission amplitude through this system as a function of the incident frequency for different thicknesses of the two-level atom slab and observe that, essentially, two modes determine the transmission spectrum. In Sec. IV, I review the Mittag-Leffler expansion, which is the mathematical tool that relates the spectral maxima with the eigenmodes of the system. In Sec. V, I compute the eigenmodes of the combined metal-two-level-atom system. These give the positions of the transmission amplitude spectral maxima and their corresponding widths. In Sec. VI, I relate the maximum of the Purcell enhancement factor to the ratio of the damping coefficient in the Drude model of the metal to the CDR of the atoms in the absence of the metals. I also establish the result that the Purcell effect enhances the CLS as well. I conclude in Sec. VII.

II. THE TRANSFER MATRIX FOR THE SYSTEM

The system being considered here consists of the following structures:

Vacuum: $z \leqslant 0$.
Metal: $0 \leqslant z \leqslant l/2$.
Two-level atoms: $l/2 \leqslant z \leqslant l/2 + \beta l$.
Metal: $l/2 + \beta l \leqslant z \leqslant l + \beta l$.
Vacuum: $z \geqslant l + \beta l$.

Using Eqs. (3.5) and (3.15) of Ref. [10], the total transfer matrix for this system is given by

$$\mathbf{M} = \mathbf{M}^{(1)} \cdot \mathbf{M}^{(2)} \cdot \mathbf{M}^{(3)} \cdot \mathbf{M}^{(4)} \cdot \mathbf{M}^{(5)} \cdot \mathbf{M}^{(6)} \cdot \mathbf{M}^{(7)}, \tag{1}$$

where

$$\mathbf{M}^{(1)} = \mathbf{M}^{B}(k,k_m) = \frac{1}{2}\left[\left(1+\frac{u_m}{u}\right)\mathbf{I} + \left(1-\frac{u_m}{u}\right)\boldsymbol{\tau}_1\right], \tag{2}$$

$$\mathbf{M}^{(2)} = \mathbf{M}^{P}\left(\tfrac{1}{2}k_m l\right) = \exp\left(i u_m \boldsymbol{\tau}_3/2\right) = \mathbf{M}^{(6)}, \tag{3}$$

$$\mathbf{M}^{(3)} = \mathbf{M}^{B}(k_m,k_{TL}) = \frac{1}{2}\left[\left(1+\frac{u_{TL}}{u_m}\right)\mathbf{I} + \left(1-\frac{u_{TL}}{u_m}\right)\boldsymbol{\tau}_1\right], \tag{4}$$

$$\mathbf{M}^{(4)} = \mathbf{M}^{P}\left(\beta k_{TL} l\right) = \exp\left(i\beta u_{TL}\boldsymbol{\tau}_3\right), \tag{5}$$

$$\mathbf{M}^{(5)} = \mathbf{M}^{B}(k_{TL},k_m) = \frac{1}{2}\left[\left(1+\frac{u_m}{u_{TL}}\right)\mathbf{I} + \left(1-\frac{u_m}{u_{TL}}\right)\boldsymbol{\tau}_1\right], \tag{6}$$

*jmanassah@gmail.com

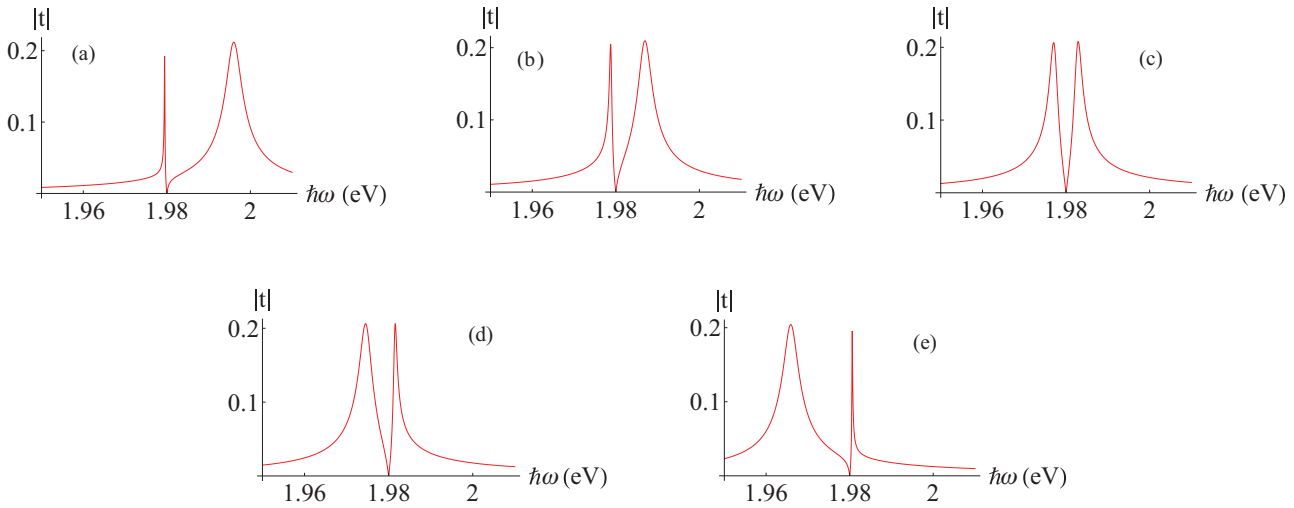

FIG. 1. (Color online) The magnitude of the transmission amplitude is plotted as a function of ω. (a) $\beta = 1.680$, (b) $\beta = 1.690$, (c) $\beta = 1.696$, (d) $\beta = 1.700$, and (e) $\beta = 1.710$. $\omega_0 = 0.22\omega_p$, $C = 10^{-6} \times \omega_p$, $\gamma_2 = 2.33\, C/4$, and $\omega_0 l/c = \pi/2$.

$$\mathbf{M}^{(7)} = \mathbf{M}^{B}(k_m,k) = \frac{1}{2}\left[\left(1+\frac{u}{u_m}\right)\mathbf{I} + \left(1-\frac{u}{u_m}\right)\boldsymbol{\tau}_1\right], \quad (7)$$

where $u = \omega l/c$, $u_m = \sqrt{\varepsilon_m(\omega)}u$, $u_{TL} = \sqrt{\varepsilon_{TL}(\omega)}u$, and

$$\boldsymbol{\tau}_1 = \begin{pmatrix} 0 & 1 \\ 1 & 0 \end{pmatrix}, \quad \boldsymbol{\tau}_2 = \begin{pmatrix} 0 & -i \\ i & 0 \end{pmatrix}, \quad \boldsymbol{\tau}_3 = \begin{pmatrix} 1 & 0 \\ 0 & -1 \end{pmatrix}, \quad \mathbf{I} = \begin{pmatrix} 1 & 0 \\ 0 & 1 \end{pmatrix}. \quad (8)$$

The matrix element $\mathbf{M}_{22}$ uniquely determines the transmission coefficient (the ratio of the outgoing field on the right to the incoming field on the left).

Using the Pauli matrices' algebra, $\mathbf{M}$ can be decomposed into the Pauli matrices' basis as follows:

$$\mathbf{M} = \Omega\mathbf{I} + [\,\Upsilon\ \cosh(2\lambda_1) + i\ \Psi\ \sinh(2\lambda_1)\,]\boldsymbol{\tau}_3 + [\Psi\ \cosh(2\lambda_1) - i\Upsilon\ \sinh(2\lambda_1)]\boldsymbol{\tau}_2, \quad (9a)$$

where

$$\Omega = \cos(u_m)\cos(u_{TL}) - \sin(u_m)\cosh(2\lambda_2)\sin(u_{TL}), \quad (9b)$$

$$\Upsilon = i[\,\sin(u_m)\ \cos(u_{TL}) + \cos(u_m)\ \cosh(2\lambda_2)\ \sin(u_{TL})\,], \quad (9c)$$

$$\Psi = \sinh(2\lambda_2)\sin(u_{TL}), \quad (9d)$$

$$\lambda_1 = \frac{1}{2}\ln\left(\frac{u}{u_m}\right), \quad (9e)$$

$$\lambda_2 = \frac{1}{2}\ln\left(\frac{u_m}{u_{TL}}\right). \quad (9f)$$

The permittivity of the noble metal (silver) is taken to be modeled by the Drude approximation as deduced from the Johnson-Christy data [11],

$$\varepsilon_m(\omega) = \varepsilon_\infty - \frac{\omega_p^2}{\omega^2 + i\Gamma\omega}, \quad (10)$$

where

$$\varepsilon_\infty^{\mathrm{Ag}} = 3.7, \quad \hbar\omega_p^{\mathrm{Ag}} = 9\ \mathrm{eV}, \quad \hbar\Gamma^{\mathrm{Ag}} = 17.28\ \mathrm{meV}.$$

The permittivity of the two-level atom medium was obtained in Ref. [3] through a full quantum-mechanical treatment and is given for the homogeneously broadened system (all Doppler effects have been neglected in this paper) by

$$\varepsilon(\omega) = 1 - \frac{C}{(\omega - \omega_0 + \omega_L) + i\gamma_T}, \quad (11)$$

where $C = 4\pi n\wp^2/\hbar$, n is the atomic number density, $\wp$ is defined such that, for a $J = 0 \to J = 1$ transition, the isolated atom decay rate is given by $\gamma_1 = \frac{4}{3}\frac{\wp^2 k_0^3}{\hbar}$, $\omega_L = \frac{C}{3}$ is the Lorentz shift, ω_0 is the isolated single atom resonant frequency, including all isolated atom QED corrections, and $\gamma_2 = (\frac{2.33}{4} + i\frac{0.22}{3})C$, which represents the effects of the short-range resonant collisions between the atoms in the binary approximation.

III. THE TRANSMISSION AMPLITUDE SPECTRAL DISTRIBUTION

To explore the characteristic features of this system, let us consider the example of an ensemble of two-level atoms with isolated atom resonance frequency given by $\hbar\omega_0 = 0.22 \times \hbar\omega_p = 1.98$ eV. I choose l to satisfy the relation $\omega_0 l/c = \pi/2$ and take $\hbar C = 9 \times 10^{-6}$ eV. In Fig. 1, I plot $|t|$ (i.e., the transmission amplitude; $|t|^2$ is the transmission coefficient) for different values of β. One notes that:

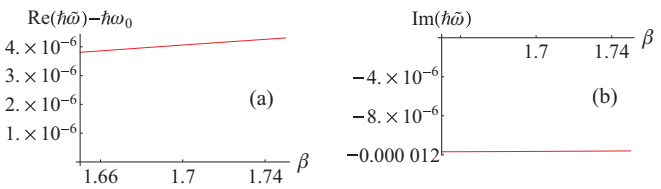

FIG. 2. (Color online) (a) The shift from ω_0 of the real part and (b) the imaginary part of the bare complex plasmonic eigenvalue for the two metallic slabs are plotted as a function of β. (All energies are in eV.) $\omega_0 = 0.22\omega_p$ and $\omega_0 l/c = \pi/2$.

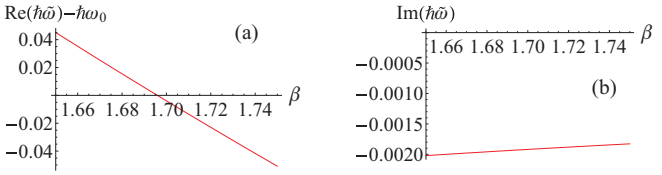

FIG. 3. (Color online) (a) The shift from ω_0 of the real part and (b) the imaginary part of the bare complex polaronic eigenvalue for the slab of two-level atoms (with no metallic slabs present) are plotted as a function of β. (All energies are in eV.) $\omega_0 = 0.22\omega_p$, $C = 10^{-6} \times \omega_p, \gamma_2 = 2.33\, C/4$, and $\omega_0\, l/c = \pi/2$.

(1) Each of the transmission amplitude curves has two peaks,

(2) for $\beta < 1.696$, the narrower peak is to the left of ω_0, whereas, it is to the right for $\beta > 1.696$, and

(3) the narrow peak increases its width as $\beta \to 1.696$, whereas, the wider peak decreases its width, until both peaks have the same width at $\beta \cong 1.696$.

My goal in the rest of this paper is to explore the underlying physics for the features observed in Fig. 1. I will find that all of the above features can directly be deduced from the values of the eigenvalues of this coupled system. These eigenvalues are those of the coupled plasmon-polariton modes of the combined metal-two-level-atom system.

It is to be noted that the coupling of the two subsystems (atoms and metals) is implemented here through imposing the continuity conditions for the tangential components of the electric field and the magnetic field at the interfaces. These boundary conditions are automatically incorporated in the transfer-matrix formalism.

IV. THE MITTAG-LEFFLER EXPANSION

I start by reviewing the basic mathematical expansion that would allow one to pursue the above analysis. Now, I summarize the Mittag-Leffler expansion [12].

Consider an expression of the form

$$f(u) = \frac{1}{(u-\omega)q(u)}, \tag{12}$$

and assume that the function $1/q\,(u)$ is meromorphic in the complex u plane, $q(u)$ has simple zeros at $\tilde{\omega}_n$, $n = 1,2,3,\ldots,$ and ω is different from any of these zeros; then the poles of $f(u)$ are all simple and are located at the zeros of $q(u)$ and at ω. Now consider a contour at infinity C_∞, and the residue

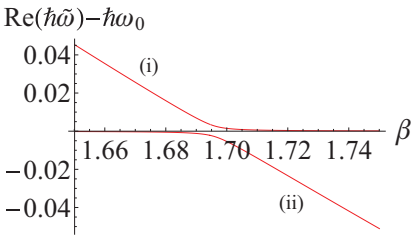

FIG. 4. (Color online) The shift from ω_0 of the real part of the interacting polariton-plasmon complex eigenvalues are plotted as a function of β. (All energies are in eV.) $\omega_0 = 0.22\omega_p$, $C = 10^{-6} \times \omega_p$, $\gamma_2 = 2.33\, C/4$, and $\omega_0\, l/c = \pi/2$.

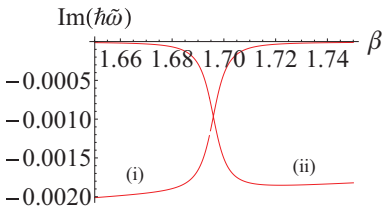

FIG. 5. (Color online) The imaginary part of the interacting polariton-plasmon complex eigenvalues are plotted as a function of β. (All energies are in eV.) $\omega_0 = 0.22\omega_p$, $C = 10^{-6} \times \omega_p$, $\gamma_2 = 2.33\, C/4$, and $\omega_0\, l/c = \pi/2$.

theorem allows one to write

$$\frac{1}{2\pi i}\oint_{C_\infty} \frac{1}{q(u)(u-\omega)}du = \frac{1}{q(\omega)} + \sum_{n=1}^{\infty} \frac{1}{q'(\tilde{\omega}_n)(\tilde{\omega}_n - \omega.)} \tag{13}$$

The contour integral vanishes if $\lim_{u\to\infty} \frac{1}{q(u)} = 0$, and consequently, the ratio $1/q\,(\omega)$ can be written in the alternative form

$$\frac{1}{q(\omega)} = \sum_{n=1}^{\infty} \frac{1}{q'(\tilde{\omega}_n)(\omega - \tilde{\omega}_n.)} \tag{14}$$

This expression is known as the Mittag-Leffler expansion, where the $\{\tilde{\omega}_n\}$'s are the complex roots of the complex expression $q(\omega) = 0$.

The above result leads one to the result that, if a plot of the function $|\mathbf{M}_{22}(\omega)|^{-1}$ has n maxima, this directly implies that $\mathbf{M}_{22}(\omega)$ has n roots in the complex plane. Thus, finding the zeros of $\mathbf{M}_{22} = 0$, also called the eigenvalues of the system, takes special importance: The real part of any of these eigenvalues corresponds to the value of ω at the corresponding maximum in $|t|$, and the imaginary part of each of these eigenvalues approximately gives the width of this maximum in the $|t|$ vs ω plot.

The reader should take special care not to confuse the eigenvalues that we will be computing with the poles of the permittivities. The latter depends only on the materials' characteristics, whereas, the former are functions of the materials' characteristics and the geometry of the system.

V. INTERACTING POLARITON-PLASMON MODES

From Fig. 1, it is clear that the combined interacting metal-two-level-atom system can be described by two active modes which are strongly coupled in the range of considered parameters.

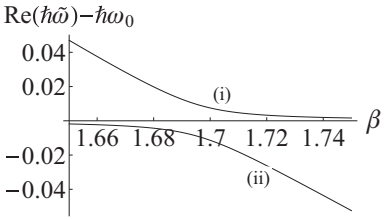

FIG. 6. The same as in Fig. 4 with all parameters being the same except that $C = 10^{-5} \times \omega_p$. (All energies are in eV.)

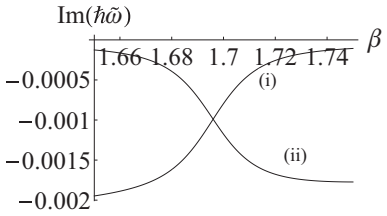

FIG. 7. The same as in Fig. 5 with all parameters being the same except that $C = 10^{-5} \times \omega_p$. (All energies are in eV.)

Consider first each of the bare modes separately, and characterize them in each of the two following configurations:

(1) isolated two metal slabs (no atoms present) and

(2) isolated ensemble of two-level atoms slab (no metal present).

In Fig. 2, I plot, for the same parameters as in Fig. 1, both the shift from ω_0 of the real part of the eigenvalue and its imaginary part as a function of β for the ensemble of atoms in the absence of the metals. Only the contributions from the collisional width [2] and from CDR and CLS are present. This is the bare polariton mode.

In Fig. 3, I plot, for the same parameters as in Fig. 1, both the shift from ω_0 of the real part of the eigenvalue and its imaginary part as a function of β for the system of the two metallic slabs in the absence of the atoms. This is the plasmon mode closest to ω_0.

In Figs. 4 and 5, respectively, I plot, for the same parameters as in Figs. 2 and 3, both the shift from ω_0 of the real part of the eigenvalues and the imaginary part of these same eigenvalues as a function of β for the two plasmon-polariton interacting systems.

One notes that for $\beta \ll 1.696$:

(1) mode (i) can be identified with the bare plasmon, and

(2) mode (ii) can be identified with the bare polaron,

whereas, the reverse is true for $\beta \gg 1.696$.

VI. PURCELL ENHANCEMENT FACTOR TO THE CDR

If we define β_{crit} as the value of β at which

$$\text{Im}[\tilde{\omega}^{(1)}(\beta_{\text{crit}})] = \text{Im}[\tilde{\omega}^{(2)}(\beta_{\text{crit}})] \tag{15}$$

(where the superscript refers to the different modes), the maximum Purcell enhancement to Dicke's CDR simply

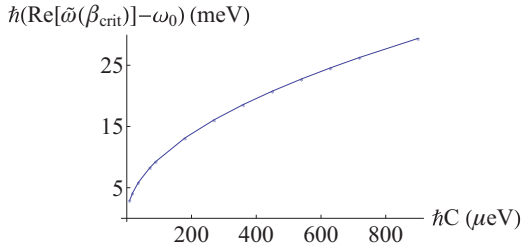

FIG. 8. (Color online) The shift at β_{crit} is plotted as a function of $\hbar C$. $\omega_0 = 0.22\omega_p$, $\beta_{\text{crit}} \cong 1.696$, $\gamma_2 = 2.33\,C/4$, and $\omega_0 l/c = \pi/2$.

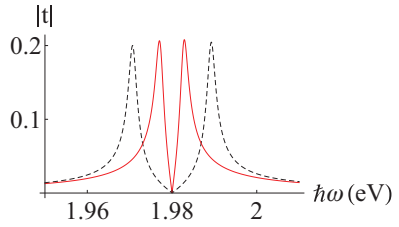

FIG. 9. (Color online) The magnitude of the transmission amplitude is plotted as a function of ω. Solid line: $C = 10^{-6} \times \omega_p$ and dashed line: $C = 10^{-5} \times \omega_p$ at $\beta \cong \beta_{\text{crit}}$. $\omega_0 = 0.22\omega_p$, $\beta = 1.696$, $\gamma_2 = 2.33\,C/4$, and $\omega_0 l/c = \pi/2$.

becomes the ratio,

$$g^{\text{Purcell}} \cong \frac{\text{Im}[\tilde{\omega}^{(2)}(\beta_{\text{crit}})]}{\text{Im}[\tilde{\omega}^{(2)}(\beta \ll \beta)]}. \tag{16}$$

I now examine the Purcell enhancement factor as the number density of the two-level atoms increases. In Fig. 6, I plot the shift in the real part of the eigenvalues from ω_0, and in Fig. 7, I plot the imaginary part of these eigenvalues for the same parameters as in Figs. 4 and 5 with only a change in the value of C. In this case, I take $\hbar C = 9 \times 10^{-5}$ eV. One notes that the value of the width of the eigenvalue at β_{crit}, the numerator of Eq. (16), approximately equals $\hbar\Gamma/2$, only changed imperceptibly (compare Figs. 5 and 7). This means that the maximum Purcell enhancement factor has decreased since the denominator of Eq. (16) has increased by a factor of 10.

Comparing Figs. 4 and 6, one notes that the separation in frequency between the real part of the two eigenfrequencies at β_{crit} has noticeably increased from Fig. 4 to Fig. 6. This shift increases as $\sqrt{C}$ when the value of $\hbar C$ is in the range of $9 \times 10^{-6} \leqslant \hbar C \leqslant 18 \times 10^{-4}$ eV. This Purcell enhancement to the CLS is discussed here. In Fig. 8, I plot this shift at β_{crit} as a function of $\hbar C$.

To verify the above theoretical predictions experimentally, one may consider measuring the transmission amplitude at β_{crit} while varying the density of the two-level atoms and/or the size of the atomic slab.

As an illustration of what one should expect if one was to vary the atomic density, in Fig. 9, I plot the magnitude of the transmission amplitude as a function of the frequency for the two values of C in Figs. 4 and 5 and that in Figs. 6 and 7 for $\beta = 1.696$. One notes that the obtained traces are in complete agreement with the predictions of the eigenmode analysis as summarized in Figs. 4–8 for the parameters specified in the respective captions. Excellent agreements are as well obtained when values of C, other than in Fig. 9, are considered (not shown in the figure).

VII. CONCLUSION

In this paper, I give the physical basis for a fuller understanding of the previously discussed Purcell-Dicke effect. This effect, which is observable when the plasmonic frequency is resonant with the atomic medium polariton frequency, can enhance the cooperative decay rate of the radiation from the ensemble of atoms that is sandwiched between the metallic plates.

Formulating this problem within the polariton-plasmon interacting modes picture gives us the means to understand, on both fundamental and quantitative bases, the reasons for having a limit on the Purcell enhancement of the cooperative decay rate and for having a nonlinear enhancement of the cooperative Lamb shift at β_{crit} in the region of saturation of the CDR.

[1] R. H. Dicke, Phys. Rev. **93**, 99 (1954).
[2] J. T. Manassah, Adv. Opt. Photon. **4**, 108 (2012).
[3] R. Friedberg, S. R. Hartmann, and J. T. Manassah, Phys. Rep. **7**, 101 (1973).
[4] J. Keaveney, A. Sargsyan, U. Krohn, I. G. Hughes, D. Sarkisyan, and C. S. Adams, Phys. Rev. Lett. **108**, 173601 (2012).
[5] H. Walther, B. T. H. Varcoe, B. O. Englert, and T. Becker, Rep. Prog. Phys. **69**, 1325 (2006).
[6] E. M. Purcell, Phys. Rev. **69**, 681 (1946).
[7] J. T. Manassah, Laser Phys. **22**, 738 (2012).
[8] R. Friedberg and J. T. Manassah, Phys. Rev. A **86**, 023804 (2012).
[9] J. T. Manassah, Chem. Phys. Lett. **544**, 73 (2012).
[10] R. Friedberg and J. T. Manassah, Phys. Lett. A **372**, 4164 (2008).
[11] P. B. Johnson and R. W. Christy, Phys. Rev. B **6**, 4370 (1972).
[12] L. Ahlfors, *Complex Analysis*, 3rd ed. (McGraw-Hill, New York, 1979).